

Transient spark: a dc-driven repetitively pulsed discharge and its control by electric circuit parameters

This article has been downloaded from IOPscience. Please scroll down to see the full text article.

2011 Plasma Sources Sci. Technol. 20 035015

(<http://iopscience.iop.org/0963-0252/20/3/035015>)

View [the table of contents for this issue](#), or go to the [journal homepage](#) for more

Download details:

IP Address: 158.195.84.207

The article was downloaded on 20/04/2011 at 07:03

Please note that [terms and conditions apply](#).

Transient spark: a dc-driven repetitively pulsed discharge and its control by electric circuit parameters

Mario Janda, Viktor Martišovič and Zdenko Machala

Division of Environmental Physics, Faculty of Mathematics, Physics and Informatics, Comenius University, Mlynska dolina F2, 84248 Bratislava, Slovakia

E-mail: janda@fmph.uniba.sk

Received 30 June 2010, in final form 10 February 2011

Published 19 April 2011

Online at stacks.iop.org/PSST/20/035015

Abstract

The paper presents an analysis of electrical characteristics of streamer-to-spark transition discharge in air at atmospheric pressure named transient spark (TS). The TS is applicable for flue gas cleaning or bio-decontamination and has potential in plasma shielding, combustion and flow control applications. Despite the dc applied voltage, TS has a pulsed character with short (~ 10 – 100 ns) high current (> 1 A) pulses, with repetitive frequencies 1–20 kHz. Estimation of the temporal evolution of electron density shows that $n_e \approx 10^{16}$ cm $^{-3}$ at maximum and $\sim 10^{11}$ cm $^{-3}$ on average are reached using relatively low power delivered to the plasma (0.2–3 W). Thanks to the high repetition frequency, n_e between two current pulses does not fall below a critical value and therefore plasma exists during the whole time. A detailed analysis of the TS control by electrical circuit parameters is presented. With appropriate circuit components, the current pulse tail (> 1 mA) can be extended and the electron density can be held above $\sim 10^{13}$ cm $^{-3}$ for several tens of μ s.

(Some figures in this article are in colour only in the electronic version)

1. Introduction

Atmospheric pressure non-thermal plasmas in air generated by electrical discharges present considerable interest for a wide range of environmental, bio-medical and industrial applications, such as air pollution control, waste water cleaning, bio-decontamination and sterilization, or material and surface treatment [1–6]. In all these applications, the desired chemical effect is achieved by efficient production of reactive radicals in non-thermal plasma. The key factors for their production are high energy electrons, which can be accelerated by electric field to reach energies of several eV, while the background gas remains cold.

The simplest approach to generating atmospheric pressure plasma is to apply a dc constant voltage on a couple of metal electrodes. If the generated electric field is not homogeneous thanks to the geometry of electrodes, e.g. pin-to-plane configuration, a gradual increase in the onset voltage will lead to the generation of corona or streamer

corona discharge [7]. Streamers are filamentary structures propagating towards the grounded electrode. Very strong reduced electric field strengths E/N (~ 600 Td) and high electron densities n_e ($\sim 10^{14}$ cm $^{-3}$) can be reached in their head [8]. Streamers can therefore significantly influence the plasma-induced chemistry. However, streamers can also lead to the transition to spark or arc discharge [7, 9], generating thermal plasma. Much more power is required to sustain these discharges. High energy costs allow their utilization only for applications where one can either expect valuable products (e.g. H $_2$) or needs to completely destroy very dangerous pollutants [10–12].

Two of the most common ways of disabling streamer-to-spark transition are based on covering at least one electrode by an insulator (e.g. dielectric barrier discharge [13–15]) or using very short high voltage (HV) pulses. We will only discuss in detail the second approach, since it is more relevant to the discharge described in this paper, which is generated between metal electrodes in point-to-plate geometry without additional insulator.

It was found that efficiency of active species formation depends on the maximum applied voltage ($10\text{--}20\text{ kV cm}^{-1}$), voltage rise time (up to 10 ns), decay time ($<1\text{--}10\ \mu\text{s}$) and total duration of the HV pulse ($<0.1\ \mu\text{s}$) [16–19]. The increasing repetition frequency of the HV pulses up to 200 Hz also showed improved efficiency of removal of various pollutants [19]. HV pulsed devices working at repetition frequencies above 1 kHz appeared only recently [20–23]. The importance of the high repetition frequency on power efficiency of the plasma generation was emphasized [21–23]. The ‘spark’ regime of nanosecond repetitive pulse discharge operating at a frequency of 30 kHz in air preheated to 1000 K, which was already successfully used for the stabilization of lean flames [24], was shown to generate plasma with a peak electron density of $\sim 10^{15}\text{ cm}^{-3}$, while consuming only 0.2–1 mJ per pulse [23]. The only disadvantage of this method could be the price of the HV pulse generator.

A restriction of thermal plasma generation when using a dc power supply can be simply achieved by adding a ballast resistor ($R > 1\text{ M}\Omega$) between the HV electrode and the dc power supply. Since R will limit the average discharge current to several mA, streamer corona will be transformed to either high pressure glow discharge (GD) or transient spark (TS), depending on the gas composition, flow rate, value of R and geometry of electrodes [25–27]. The high pressure GD has already been applied, e.g. for flue gas cleaning [25, 28], and it has great potential for other applications, such as plasma shielding, since it is a source of stable scalable plasma where $n_e \approx 10^{12}\text{ cm}^{-3}$ can be achieved. The TS discharge regime was first mentioned in [25] and further described in [27]. It has also been successfully applied for several environmental and bio-medical applications [5, 25, 29].

TS is a relatively new type of discharge, yet its concept is similar to the prevented spark studied by the group of Marode [30–32]. Periods with TS were also observed by Akishev *et al* [33], while studying instabilities of GD due to a fast gas flow. TS is a filamentary streamer-to-spark transition discharge initiated by a streamer, which transforms to a short spark pulse due to the discharging of the internal capacitance C of the reactor. TS is based on charging and discharging of C . For typical R and C ($\sim 10\text{ pF}$), a repetition frequency of this process 1–20 kHz can be achieved. TS represents a simple solution to generate short ($\sim 10\text{--}100\text{ ns}$) high current pulses ($\sim 1\text{--}10\text{ A}$) with high repetition frequency ($\sim\text{kHz}$). Thanks to the short current pulse duration, the plasma generated by TS has different properties than the plasma generated by an ordinary spark. Our previous time-integrated emission spectroscopy study showed that TS pulses generate highly reactive non-equilibrium plasma with excited atomic radicals (O^* , N^*), excited molecules N_2^* and ions N_2^{+*} and gas temperature T_g ranging from 500 to 1500 K, while vibrational temperature T_v was about 3800–5000 K [5]. In comparison with an ordinary spark (or even high pressure GD) TS has also a relatively low power budget: the discharged energy in one TS pulse is small ($\sim 0.1\text{--}1\text{ mJ}$) and the total power, depending on pulse frequency, is 0.1–2 W [5, 25].

Thanks to these characteristics, TS is not applicable where heating to even just about 500 K can be harmful, e.g. for

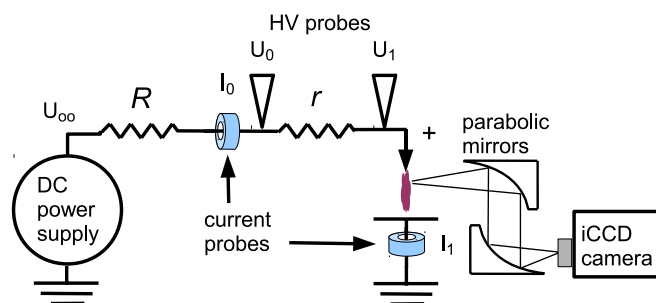


Figure 1. Simplified scheme of the experimental set-up.

treatment of heat sensitive solid materials, but is applicable for flue gas cleaning or bio-decontamination, and has potential in plasma shielding, combustion and flow control applications. Various applications have different demands on TS with respect to the optimal frequency, energy per pulse, etc. So the optimization of TS for various applications and better ability to control it by changing electric circuit parameters requires further research.

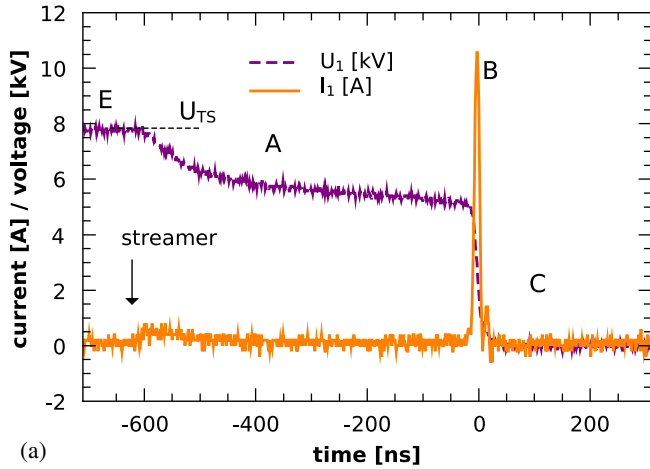
2. Experimental set-up

Figure 1 shows a simplified scheme of the experimental set-up. Experiments were carried out at room temperature in atmospheric pressure air with a gas flow perpendicular to discharge channel with a velocity of $\sim 0.2\text{ m s}^{-1}$. A stainless-steel hypodermic needle ($20\text{G} \times 1\frac{1}{2}''$, $0.9 \times 40\text{ mm}$) with standard bevel was used as a HV electrode opposite a grounded planar copper electrode. The distance between electrodes $d = 5\text{ mm}$.

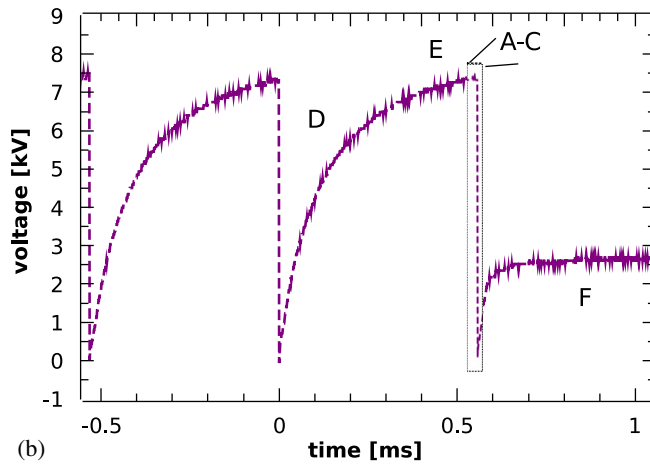
A dc high voltage (HV) power supply connected via a series resistor R limiting the total current was used to generate a positive TS discharge. The value of R varied from 3.5 to 9.84 M Ω . An additional small resistor r , the effect of which we further studied, was attached directly to the HV electrode, separating it thus from a HV cable connecting it with the resistor R (figure 1). The value of r varied from 0 (no r) to 110 k Ω .

The discharge voltage was measured by two 100 M Ω HV probes (Tektronix P6015A) at both ends of the resistor r . We emphasize here its presence and position because it has an influence on TS properties. The length of the HV cable between the resistor R and the HV electrode can significantly contribute to the total capacity C discharging during each TS pulse. We tested different cables with lengths from 0.3 to 2 m, having capacities from approximately 5–34 pF. The currents at the grounded electrode and between R and r were measured by a Pearson Electronics 2877 (1V/A) and a Pearson Electronics 4100 (1V/A) current probes. All current and HV probes were linked to the 200 MHz digitising oscilloscope Tektronix TDS2024 with a sampling rate up to 2 Gs s^{-1} .

Images of single TS pulses were taken by an intensified CCD camera (Andor Istar) with a time resolution down to 2 ns, in order to estimate the diameter of generated plasma channels. The iCCD camera was triggered by a generator of 5 V rectangular pulses, which was triggered directly by the



(a)



(b)

Figure 2. Typical waveforms of TS on (a) ns time scale, (b) ms time scale, $R = 6.5 \text{ M}\Omega$, $f \approx 2 \text{ kHz}$, $r = 0 \text{ }\Omega$, $C = 43 \pm 4 \text{ pF}$, $d = 5 \text{ mm}$, TS pulse parameters: FWHM $\approx 12 \text{ ns}$, rise and decay time $\sim 5 \text{ ns}$.

current signal. For this purpose we measured the discharge current also on a $50 \text{ }\Omega$ or $1 \text{ }\Omega$ resistor shunt. This enabled us to synchronize the acquisition of the emission either with the beginning of the streamer or with the beginning of the spark, depending on the resistor shunt used. However, in both cases we are unable to acquire the initial 25 ns of emission due to a delay caused by the trigger generator, transmission time of the signal by BNC cables and a camera insertion delay.

3. Results and discussion

3.1. Introduction to transient spark

When the high voltage U_0 applied to the stressed electrode is progressively increased, we first observe a streamer corona. When the breakdown voltage is reached, a transition to TS occurs at the discharge voltage U_{TS} . TS is a filamentary streamer-to-spark transition discharge initiated by a streamer, which transforms to a short spark pulse (phase B, figure 2(a)). The duration of the streamer-to-spark transition period (phase A, figure 2(a)) is from ~ 0.1 to $1 \text{ }\mu\text{s}$, depending on TS repetition frequency [34]. Figure 3 shows a typical TS.



Figure 3. Photograph of TS in positive needle-plane gap of 4 mm, $f = 2 \text{ kHz}$, $R = 6.6 \text{ M}\Omega$ and exposure 0.05 s.

The TS current pulse is due to the discharging of the capacity C , composed of several components (internal capacity of the discharge chamber C_{int} , capacity of the HV cable C_{cable} between the ballast resistor R and the electrode and capacity of the HV probe $C_{\text{HV}} = 3 \text{ pF}$). When C is discharged, the current, approximately given by

$$I_1(t) \approx -C \frac{dU_1(t)}{dt}, \quad (1)$$

reaches a high value ($\sim 1 \text{ A}$) and the voltage drops to almost zero (phase C, figure 2(a)). Then, during the quenched phase (phase D, figure 2(b)), C is recharged by a growing potential U_1 on the stressed electrode. The growth of the potential U_1 in time t can be in a first approximation described by the following equation:

$$U_1(t) = U_0 \left[1 - \exp\left(\frac{-t}{RC}\right) \right]. \quad (2)$$

Usually, during this relaxation phase when the gap potential reaches a specific threshold, corona discharge appears, and some pre-breakdown streamers (phase E, figures 2(a) and (b)). A new TS pulse occurs in time $t = T$, when the voltage at the HV electrode U_1 reaches the breakdown voltage to TS U_{TS} (figure 2(a)), given according to (2) by

$$U_{\text{TS}} = U_0 \left[1 - \exp\left(\frac{-T}{RC}\right) \right]. \quad (3)$$

From (3) we obtain the characteristic repetition frequency f of this process:

$$f = \frac{1}{T} = \frac{1}{RC \ln \left[\frac{U_0}{(U_0 - U_{\text{TS}})} \right]}. \quad (4)$$

However, the repetition frequency f of the first TS pulses, when U_0 only slightly exceeds U_{TS} is low and very irregular (figure 4(a)). Further increase in U_0 leads to an increase in f and TS pulses become more regular (figure 4(b)). For typical

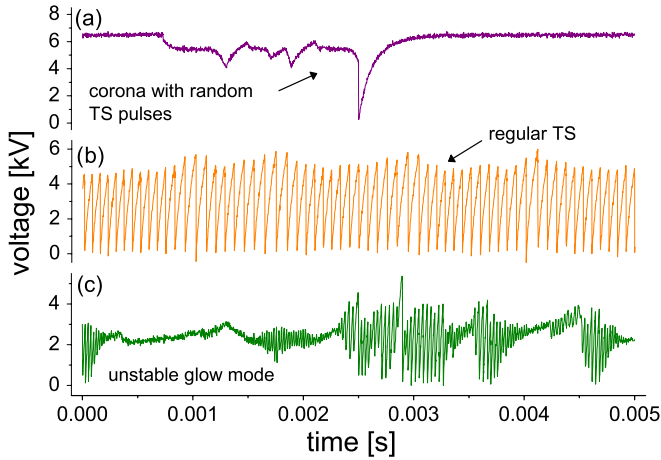


Figure 4. Voltage waveforms of different discharge regimes: (a) the first random TS pulses, (b) regular TS and (c) the unstable glow mode [37].

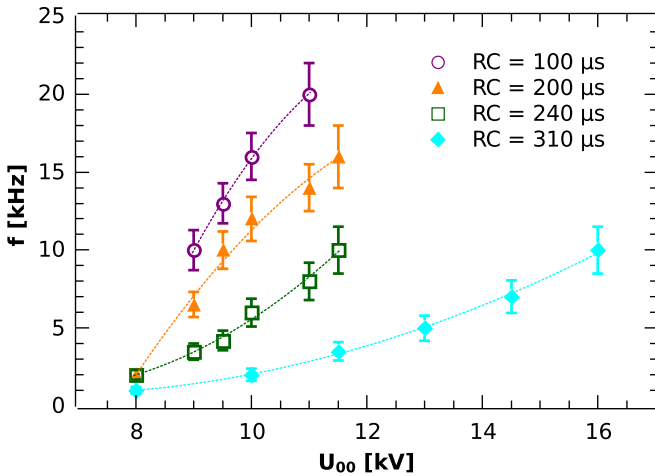


Figure 5. The dependence of f on the onset voltage U_{00} for several RC values, $r = 0 \Omega$ and $d = 5$ mm.

R and C , the repetition frequency f is in the order of several kHz and grows with increasing U_{00} (figure 5). However, even with known values of C and R , formula (4) is not reliable to predict the growth of f with U_{00} , because U_{TS} also depends on f (figure 6). The decrease in U_{TS} with f can be explained by the increasing gas temperature T_g , resulting in decreasing gas density N . From some threshold, the reduced electric field E/N is sufficient to initiate the TS pulse, E and thus also U_{TS} can be lowered [34].

The actual value of U_{TS} depends also on other parameters, the most important ones being the gap length and the sharpness of the HV electrode. In our case, it is difficult to describe the shape of the HV needle electrode geometrically. In the first approximation, its tip can be considered as a hyperboloid surface with the radius of curvature ϕ . Although we did not accurately measure ϕ in our experiments, it is safe to say that it was between $100 \mu\text{m}$ and 1 mm. More importantly, TS does not significantly influence the shape of the tip. On the other hand, oxidation of the plane electrode has a more important influence on the TS properties. It was therefore necessary to regularly clean its surface in order to obtain reproducible results.

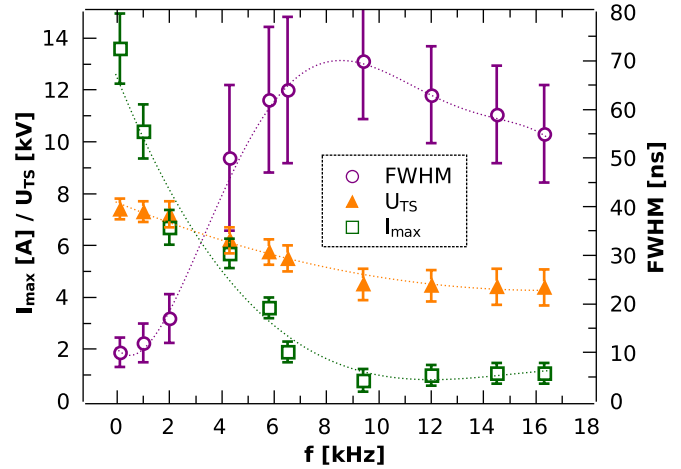


Figure 6. The dependence of peak current (I_{\max}), breakdown voltage U_{TS} and FWHM of current pulses on f , $C = 32 \pm 4$ pF, $R = 6.6 \text{ M}\Omega$, $r = 0 \Omega$ and $d = 5$ mm.

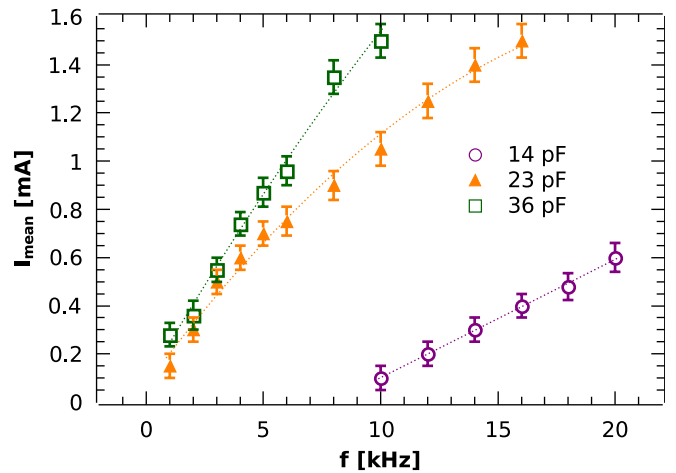


Figure 7. The dependence of mean discharge current I_{mean} on f , $R = 6.6 \text{ M}\Omega$, $r = 0 \Omega$ and different values of C .

3.2. TS control by electric circuit parameters

The RC term determines which frequencies can be achieved and how fast f grows with U_{00} (figure 5), but R and C also influence other TS properties. The major role of R is to avoid the transition to arc or the GD, because increase in f is accompanied by increase in mean current I_{mean} (figure 7). As I_{mean} exceeds approximately 1.5 mA, TS tends to transform into a pulse-less GD regime with a constant current up to 2 mA (phase F, figure 2(b)). However, due to the high value of R and the electro-negativity of air, this regime is not stable and the discharge randomly switches between the glow regime and the high frequency TS regime (figure 4(c)). Typically, R should be above $5 \text{ M}\Omega$ to avoid transition to a stable GD. On the other hand, if $R > 10 \text{ M}\Omega$, the energy losses on the external resistor become too high for operating at high f and therefore also high I_{mean} . Even for $R = 6.6 \text{ M}\Omega$, the power dissipated in this external resistor exceeds the power input to plasma for $I_{\text{mean}} > 0.6$ mA (figure 8). So the TS properties cannot be controlled by changing the value of R alone.

The influence of C on TS is even more significant. Since TS is based on charging and discharging of C , total charge

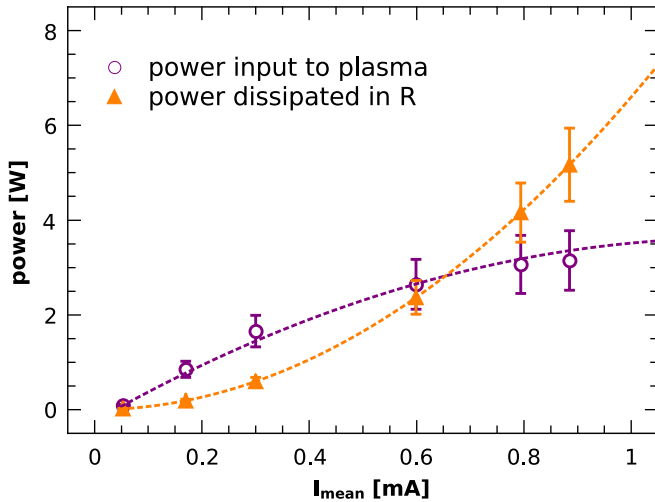


Figure 8. Comparison of the power input to plasma with the power dissipated in external resistor, $R = 6.6 \text{ M}\Omega$, $r = 0 \text{ }\Omega$ and $C = 32 \pm 4 \text{ pF}$.

Q_p and the energy delivered to the discharge gap per pulse E_p are functions of C . We can therefore affect the shape of TS current pulses by changing C . Larger C typically means larger current pulses. However, we must also take into account the dependence of the current pulse maximum I_{\max} and current pulse width (FWHM) on f . With increasing f , pulses become smaller and broader (figure 6). The increase in I_{\max} with increasing C is therefore observed only at constant f .

However, the question is how to control C ? It consists of several components, from which one can easily change only the value of C_{cable} by changing the cable length. Longer cable means larger C_{cable} . However, it is not very practical to change C using different HV cables with various lengths. So we use long cables ($C_{\text{cable}} > 20 \text{ pF}$) and place a small separating resistor r between the HV electrode and HV cable. This r separates C_{cable} from $C_{\text{int}} + C_{\text{HV}}$. Like this, we were able to control the shape of the current pulse by changing r , without changing C_{cable} .

3.3. The influence of separating resistance r on TS

We expected that the increasing value of r would lead to a gradual decrease in I_{\max} . This tendency was experimentally confirmed (figure 9), but the dependence of the pulse shape and width on r was not the expected monotonic increase. We found that FWHM is not a proper parameter to describe TS pulses, since they are obviously formed by a convolution of two independent current pulses (figure 10). The first one (I_{C_1}) is due to discharging of the capacitance $C'_1 = C_{\text{int}} + C_{\text{HV}}$ in the gap. The second one (I_0) is due to discharging of the HV cable through the resistor r .

These two currents, I_{C_1} and I_0 , can explain the dependences of I_{\max} and pulse shape on r . While I_{C_1} does not change significantly with r (figure 9, 1st peak), I_0 becomes smaller (figure 9, 2nd peak) and broader. As a result, I_{\max} also decreases with r , but when the maximum of I_0 becomes small compared with the maximum of I_{C_1} , I_{\max} remains almost

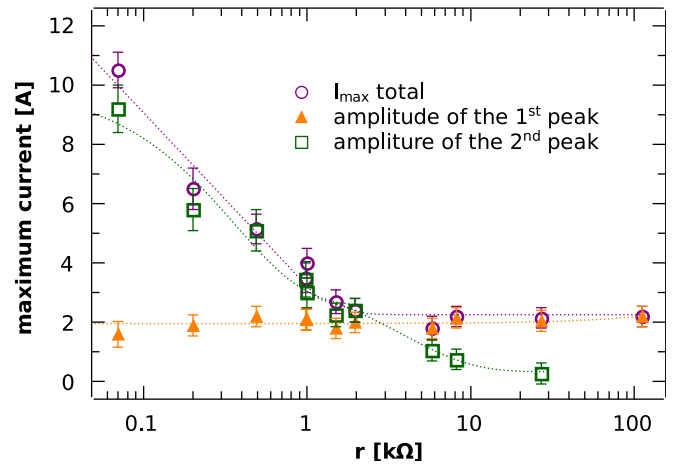


Figure 9. The influence of separating r on the amplitude of TS current pulse, and its two components, $R = 9.84 \text{ M}\Omega$, $f \approx 1.1 \text{ kHz}$, $C = 43 \pm 4 \text{ pF}$.

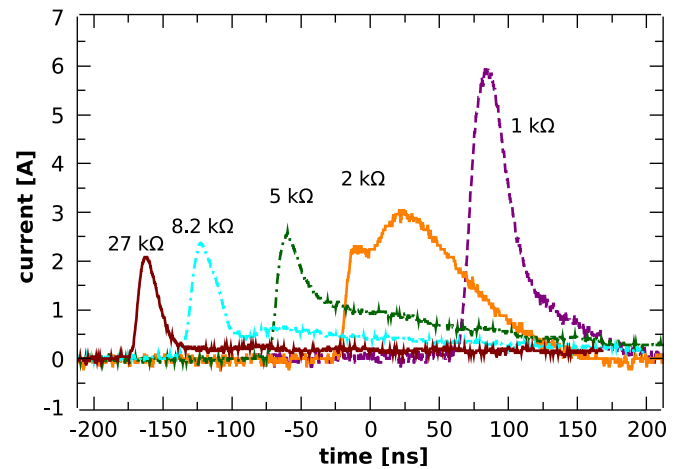


Figure 10. The influence of separating r on the shape of TS current pulses, $R = 9.84 \text{ M}\Omega$, $f \approx 1.1 \text{ kHz}$ and $C = 43 \pm 4 \text{ pF}$.

constant for a further increase in r (figure 9, $r > 10 \text{ k}\Omega$). Here we obtained I_0 from I_1 after subtraction of I_{C_1} . C'_1 necessary to calculate I_{C_1} was obtained by fitting measured current waveforms by (5) for large r .

We expected that I_0 can also be derived from the measured potential drop on r :

$$I_1(t) \approx I_{C_1} + I_0 = -C'_1 \frac{dU_1(t)}{dt} + \frac{U_0 - U_1}{r}. \quad (5)$$

We experimentally tested the validity of (5) by measuring current I_0 flowing through r (figure 11). However, the agreement between the measured current and the current calculated from U_0 and U_1 was good enough only for $r > 1.5 \text{ k}\Omega$. For smaller r , experimental results were in agreement only with I_0 derived from I_1 after subtraction of I_{C_1} . In order to find a better formula for $I_1(t)$, which would enable us to calculate it from the measured voltage waveforms for all values of r , we performed a detailed analysis of the electric circuit representing our experimental set-up.

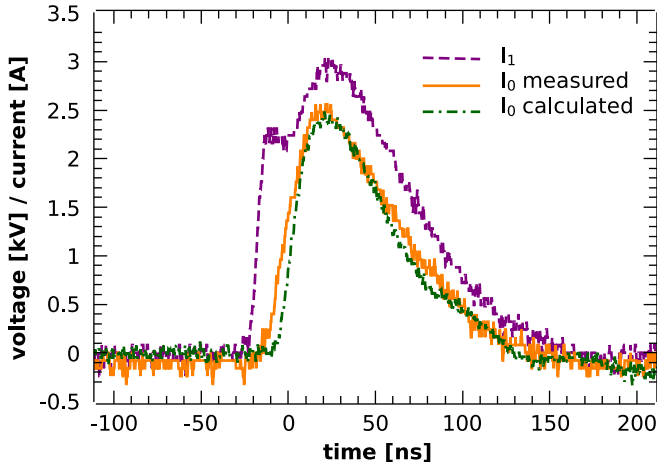


Figure 11. Comparison of I_0 measured by the current probe with I_0 calculated from U_0 and U_1 , $r = 2 \text{ k}\Omega$, $C = 43 \pm 4 \text{ pF}$ and $C'_1 = 7 \pm 1 \text{ pF}$.

3.4. Analysis of the electric circuit representing TS

Figure 12 shows a simplified electric circuit representing TS. Here, the separating resistor is characterized not only by its resistance r but also by its inductance L_0 . We found it to be crucial to explain the observed oscillations of the measured current and voltage waveforms. We even have to include the inductance L_1 of the cable from the planar low voltage electrode to ground. For this reason we also had to divide C_{int} into two parts. The first one, C_{el} , represents the capacity of electrodes. The second one is included in C_1 .

The utilization of the HV probes also introduces a resistance $R_{\text{HV}} = 100 \text{ M}\Omega$ through which parasitic loss currents pass. The capacity of these probes is included in C_0 and C_1 , respectively. The discharge plasma is represented by its resistance R_p . The plasma resistance is unknown and changes in time. This is the parameter responsible for the pulsed character of TS. If we know R_p , we would be able to describe all parameters of this circuit (U_1 , I_1 , ...) from the voltage and the current provided by the HV power supply. In contrast, from the measured values of U_0 , U_1 and I_1 we can derive the time variations of R_p . From R_p , we can estimate the plasma conductivity and thus the electron density.

First of all, let us find the dependence of I_1 on U_0 and U_1 starting from the basic equations describing the electric circuit

$$I_1 = I_0 - \frac{U_1}{R_{\text{HV}}} - C_1 \frac{dU_1}{dt}, \quad (6)$$

$$U_1 = U_0 - rI_0 - L_0 \frac{dI_0}{dt}. \quad (7)$$

If r is sufficiently high compared with L_0 , the third term in (7) can be neglected and from combination of (6) and (7) we obtain

$$I_1(t) = -C_1 \frac{dU_1(t)}{dt} + \frac{U_0 - U_1}{r} - \frac{U_1}{R_{\text{HV}}}. \quad (8)$$

This is actually equivalent to equation (5), corrected by the current lost through R_{HV} . If L_0 can be neglected, C_1 becomes equal to C'_1 , because C_{el} can now be added to C_1 . If the

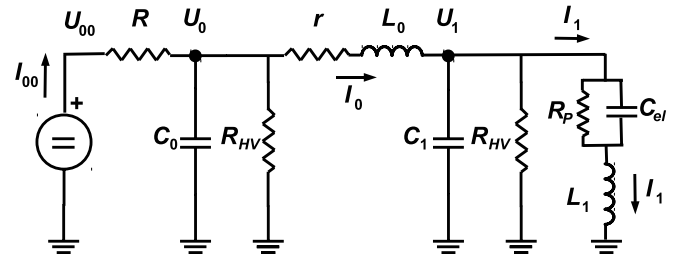


Figure 12. A simplified electric circuit representation of TS.

inductance term in (7) cannot be neglected, we must use another equation obtained from the analysis of the circuit:

$$I_0 = I_{00} - \frac{U_0}{R_{\text{HV}}} - C_0 \frac{dU_0}{dt}, \quad (9)$$

where

$$I_{00} = \frac{U_{00} - U_0}{R}. \quad (10)$$

From the combination of (6) and (9) we obtain

$$I_1 = \frac{U_{00} - U_0}{R} - \frac{U_0 + U_1}{R_{\text{HV}}} - C_0 \frac{dU_0}{dt} - C_1 \frac{dU_1}{dt}. \quad (11)$$

The first term is feeding current from the power supply, the second one is current lost through R_{HV} . During the TS high current pulse (phase B), these two terms are negligible, but they are important to estimate the current during phases C and E. The last two terms of (11) dominate during phase B and they correspond to two current terms in (5), but they are now both expressed as capacitive currents. Capacitance C_0 is the sum of C_{cable} and C_{HV} of the second HV probe. Validity of this formula was again checked by fitting the measured waveforms of I_1 and I_0 . For the longest 2 m HV cable we thus obtained values of $C_0 = 37 \pm 3 \text{ pF}$ and $C_1 = 7 \pm 1 \text{ pF}$, which could be used to obtain I_1 from U_0 and U_1 for every value of r .

However, the problem of (11) is that it does not directly describe the dependence of TS parameters on r , which is not even included there. Moreover, we also wanted to find relations between U_0 , U_1 and I_1 , which would enable us to reduce the number of parameters we have to measure during the experiments. In order to reduce the number of required HV probes, we need to describe U_1 as a function of U_0 . We can obtain it after we add the derivative of (9) to (7):

$$U_1 = (1 + r\rho)U_0 - \frac{r}{R}U_{00} + (rC_0 + \rho L_0) \frac{dU_0}{dt} + L_0 C_0 \frac{d^2 U_0}{dt^2}, \quad (12)$$

where

$$\rho = \frac{R + R_{\text{HV}}}{R_{\text{HV}}R}. \quad (13)$$

Here we could neglect the term with the derivative of U_{00} . Finally, from the combination of (11) and (12) we obtain the dependence of I_1 on U_0 , which also directly includes the influences of r , C_0 , C_1 and L_0 :

$$I_1 = c_{00} U_{00} + c_0 U_0 + c_1 \frac{dU_0}{dt} + c_2 \frac{d^2 U_0}{dt^2} + c_3 \frac{d^3 U_0}{dt^3}, \quad (14)$$

where

$$c_{00} = \frac{r + R_{HV}}{R_{HV}R}, \quad (15)$$

$$c_0 = -\frac{rR + rR_{HV} + 2R_{HV}R + R_{HV}^2}{RR_{HV}^2}, \quad (16)$$

$$c_1 = -C_0 - (1 + r\rho)C_1 - \frac{rC_0}{R_{HV}} - \frac{\rho L_0}{R_{HV}}, \quad (17)$$

$$c_2 = -rC_1C_0 - \rho C_1L_0 - \frac{L_0C_0}{R_{HV}} \quad (18)$$

and

$$c_3 = -L_0C_1C_0. \quad (19)$$

The validity of (12) and (14) was also tested and confirmed by fitting measured waveforms. With equation (14), it is no longer necessary to use two HV probes. However, it is crucial to measure U_0 with very low noise level, otherwise its triple numerical derivative would lead to large error. In such a case, this equation is only useful to estimate the background and parasitic currents (first two terms).

3.5. Estimation of the plasma resistance and electron density

We can use the dependence of the electron number density on the plasma conductivity σ_p to calculate n_e :

$$n_e = \frac{\sigma_p m_e \nu_c}{e^2}. \quad (20)$$

Here e and m_e are the electron charge and mass, respectively, and ν_c is the electron–heavy particles collision frequency. The plasma conductivity σ_p is related to the plasma resistance R_p by

$$\sigma_p = \frac{d}{R_p A}, \quad (21)$$

where d and A are the gap length and the cross-sectional area of the plasma channel, respectively.

A formula describing the dependence of R_p on the discharge voltage and current can be obtained by an analysis of the electric circuit representing TS. We obtain

$$R_p = \frac{U_1 - L_1 \frac{dI_1}{dt}}{I_1 - C_{el} \frac{dU_1}{dt} + L_1 C_{el} \frac{d^2 I_1}{dt^2}}. \quad (22)$$

From this equation, R_p can be calculated if we know the values of L_1 and C_{el} . We minimized the influence of L_1 using the shortest possible grounding wires (~ 10 cm), with estimated inductance ~ 100 nH. For this reason, the influence of L_1 is not negligible only for very sharp high current pulses ($I_{\max} > 5$ A and pulse width ~ 10 ns) with a large derivative of I_1 . These high pulses appear only at frequencies below 2 kHz, if the total capacity of the system $C > 20$ pF and if the separating resistor r is very small ($r < 0.5$ k Ω). For all estimates of R_p presented here, therefore, the influence of L_1 can be neglected. This means that the term $C_{el} \frac{dU_1}{dt}$ can also be neglected, because without L_1 , C_{el} can be added to C_1 and I_1 is equal to I_p .

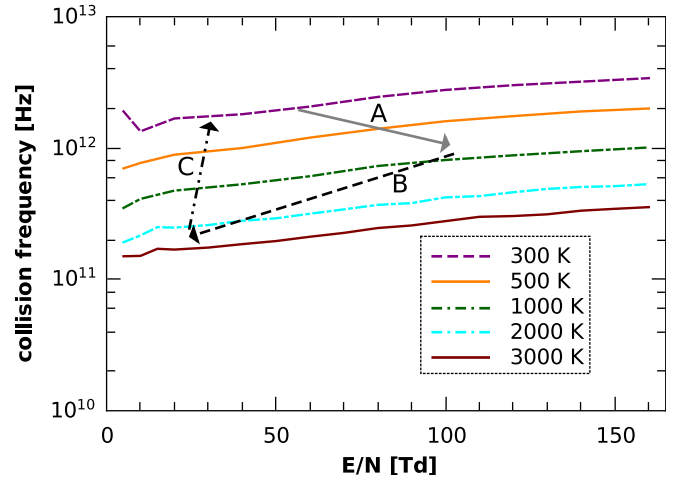


Figure 13. Collision frequency of electrons with neutrals as a function of T_g and E/N , arrows represent estimated changes in ν_c during different phases of TS, A—streamer-to-spark transition phase, B—short spark pulse and C—phase after the spark.

Under these simplifications, we can estimate R_p directly from the measured U_1 and I_1 , but we also used (14) to better estimate I_1 before and after the high current pulse. Moreover, U_1 is not measured accurately enough by the HV probe at the beginning of phase B of TS, when it falls to very low values. For this reason, we estimated R_p also from I_0 and U_0 , because U_0 does not drop to very low values for $r > 1.5$ k Ω . When C_1 is already discharged, the following equation can be used:

$$R_p = \frac{U_0}{I_{00} - \frac{U_0}{R_{HV}} - C_0 \frac{dU_0}{dt}} - r. \quad (23)$$

In addition to the uncertainty of R_p , the plasma diameter D_p , necessary to calculate A , and ν_c , are other major sources of uncertainty in the estimation of n_e . We calculated ν_c in air for T_g from 300 to 3000 K and for E/N from 10 to 200 Td (figure 13) using our package for Monte Carlo simulation of electron dynamics [35]. We found that within this region of T_g and E/N , the value of ν_c can vary from approximately 2×10^{11} to 4×10^{12} s $^{-1}$. Since both T_g and E/N certainly change during the evolution of TS, ν_c must change as well. Based on our preliminary results [34], we can roughly describe the time evolution of T_g and E/N . The resulting evolution of ν_c is depicted in figure 13 by arrows. Arrow A represents the streamer-to-spark transition phase with an initial temperature 300–400 K and E/N around 50 Td. The increase in T_g up to ~ 1000 K was observed during this phase before transition to spark. If the pressure remains constant, this would result in the increase in E/N up to ~ 150 Td, due to the decrease in the gas density. However, the increase in pressure cannot be neglected here. We are not able to measure it now, but based on calculations of Naidis [36] we assume that the increase in E/N during phase A is smaller, up to ~ 100 Td. Changes in ν_c during the spark phase of TS are represented by the arrow B (figure 13). Here we assume further increase in T_g , up to ~ 2500 K at least [34], and the drop in E/N to small values. After discharging the internal capacitance of the system, during

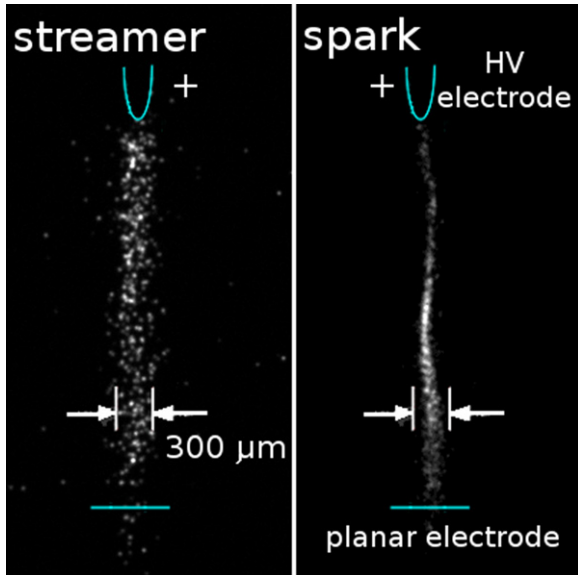


Figure 14. Images of the streamer and spark of a single TS pulse taken by iCCD camera, exposure 25 ns, acquisition started ~ 25 ns after the beginning of the streamer and spark, respectively, $r = 0.9$ k Ω , $f \approx 2$ kHz, $R = 6.6$ M Ω , $C = 32 \pm 4$ pF and $d = 4$ mm.

phase C, the temperature decreases and E/N grows slowly (arrow C, figure 13). We are not able to describe changes in v_c more precisely right now, so we use the constant value 10^{12} s $^{-1}$. This approximation introduces an uncertainty of less than a factor of 4.

In order to obtain an estimate of D_p , we made an assumption that the plasma diameter can be well defined by the volume from which emission can be observed. We therefore performed a set of experiments of TS imaging by iCCD camera (see figure 14 for illustration), during which we varied the repetition frequency of TS. The iCCD camera was triggered directly by the current signal and we were able to synchronize it either with the beginning of the streamer or the spark event. We found that D_p of a plasma channel generated by a streamer is approximately 300 μm . The subsequent spark channel is narrower (at least for $f < 4$ kHz), probably even slightly less than 100 μm , but it slightly expands close to the planar electrode. The contraction of the plasma channel is in agreement with the calculations of Naidis [36]. Despite the fact that we were able to obtain images of different phases of TS, we were not able to obtain the whole time evolution of D_p . First of all, we cannot see the initial 25 ns of the light emission because of the triggering issue (see section 2). Next, the emission is not strong enough during the whole streamer-to-spark transition phase, and more than around 100 ns after the spark phase. However, the later phase of TS with current around 1 mA is similar to a GD. The diameter of a stable GD channel is around 500 μm [5], and we suppose that this value can be used in the first approximation as the upper limit of TS plasma channel diameter. Finally, we decided to use a single value of plasma channel diameter $D_p = 200$ μm . This approximation introduces an uncertainty less than a factor of 3 for phases A–C of TS, after the establishment of conductive plasma channel by streamer preceding the TS pulse. Altogether, we can estimate

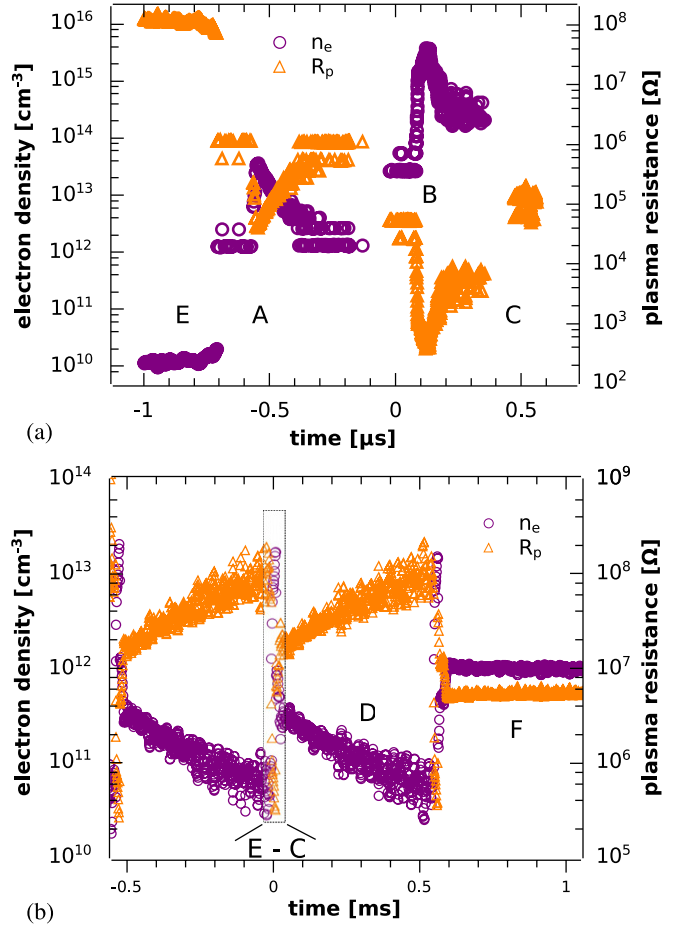


Figure 15. Calculated electron density and plasma resistance during a TS pulse on (a) μs time scale, (b) ms time scale, $f \approx 2$ kHz and $C = 32 \pm 4$ pF.

n_e with not better than an uncertainty factor of 10, for these phases. It is questionable whether we can approximate the plasma by a column also in later phases D and E. Even if yes, its expansion should be included. Values of n_e estimated for these phases are therefore only informative.

Figure 15 shows a typical time evolution of R_p and n_e for TS with no separating resistor r and a repetition frequency of ~ 2 kHz on two different time scales. Figure 15(a) is a zoom on the high current phase of TS, whereas figure 15(b) shows the estimate of R_p and n_e during several TS cycles. As we can see, the initial n_e , even before bridging of the gap by a streamer, is relatively high. Values from around 10^{10} – 10^{13} cm $^{-3}$ were observed, though this value is only informative, as was mentioned above. This high concentration can be explained by preliminary streamers and corona discharge phase of TS. During the short spark pulse, R_p drops to a few hundred ohms and n_e can reach $\sim 10^{16}$ cm $^{-3}$. As soon as C is discharged, n_e drops quickly to about 10^{14} cm $^{-3}$. After the TS pulse, n_e gradually decreases to about 10^{10} – 10^{11} cm $^{-3}$ (figure 15(b)). In reality it should be lower, because we did not include the expansion of plasma channel in this estimation. However, even if the volume of plasma expands by two orders of magnitude (average diameter 2 mm), the lowest n_e would be in the order of 10^8 – 10^9 cm $^{-3}$. In this case, the Debye length would be not larger than 0.2 mm (calculated for $T_e = 1000$ K and

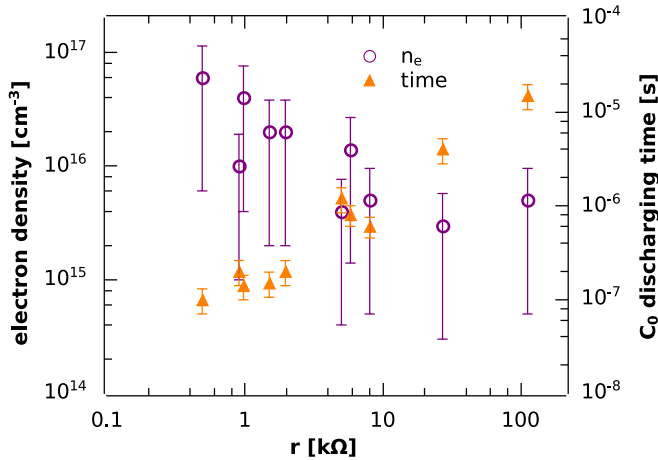


Figure 16. Dependence of maximum electron density and C_0 discharging time on r , $R = 9.84 \text{ M}\Omega$, $f \approx 2 \text{ kHz}$, $C_0 = 37 \pm 3 \text{ pF}$ and $C_1 = 7 \pm 1 \text{ pF}$.

$n_e = 10^8 \text{ cm}^{-3}$) which is one order of magnitude smaller than the assumed plasma dimension. We can therefore suppose that plasma exists during the whole period of TS, even during the relaxation phase, although its resistance becomes quite high ($R_p \sim 10^8 \text{ M}\Omega$).

Figure 15(b) also shows a short period of the unstable GD regime and for this period we obtained $n_e \approx 10^{12} \text{ cm}^{-3}$. This is in very good agreement with previous studies of GD [5], where n_e was estimated from the current density. This fact confirms that our calculated values of n_e are reasonable.

3.6. Influence of r on R_p and n_e

Increasing value of r leads to a decrease in I_{max} and therefore also to lower maximum n_e (figure 16). On the other hand, increasing r causes it to take longer for C_0 to be discharged—up to $\sim 20 \mu\text{s}$ for $r = 111 \text{ k}\Omega$ (figure 16). This prolongation of the current tail means that n_e stays relatively high longer. Typical n_e at the end of discharging of C_0 was $\sim 10^{13} \text{ cm}^{-3}$. We also estimated that it takes up to $\sim 100 \mu\text{s}$ ($r = 111 \text{ k}\Omega$) for n_e to drop below $\sim 10^{12} \text{ cm}^{-3}$. Thus, higher r enables us to merge the characteristics of TS and GD together, i.e. relatively high current pulse ($\sim 2 \text{ A}$) with high efficiency of production of radicals are followed by a long period with current above 1 mA , during which plasma reaches characteristics typical for GD.

On the other hand, the voltage U_0 does not drop to low values for larger r , e.g. for $r = 27 \text{ k}\Omega$, $U_0^{\text{min}} \approx 1.5 \text{ kV}$, and so C_0 cannot be discharged completely. It is therefore not suitable to use larger values of r . The separating resistor r must remain much smaller than the ballast resistor R , otherwise the discharging of C_0 has negligible effect on the discharge current and $r + R$ can be treated as one resistor.

4. Conclusions

A new concept of a dc-driven pulsed discharge was investigated: TS, a repetitive streamer-to-spark transition discharge of very short pulse duration (~ 10 – 100 ns) and with very limited energy so that the generated plasma is highly

non-equilibrium. This discharge can be maintained at low energy conditions (up to 1 mJ/pulse) by an appropriate choice of the resistances and capacitances in the electrical circuit, and its frequency can be controlled by the applied voltage. The activity of TS is comparable to the nanosecond repetitive pulsed discharges but its advantage is the ease of the dc operation and no need for special and expensive HV pulsers with high repetition frequency and nanosecond rise times.

Our calculations of temporal evolution of electron density in TS based on the detailed analysis of the electrical circuit showed that $n_e \approx 10^{16} \text{ cm}^{-3}$ at maximum and $\sim 10^{11} \text{ cm}^{-3}$ on average are reached. Better estimation of these values will require further time-resolved emission spectroscopic study and imaging with fast iCCD camera coupled to a monochromator in order to estimate the evolution of plasma dimensions and the gas temperature inside the plasma. These investigations are in progress and will be a subject of the following paper.

The influence of a resistor r separating the HV cable from the HV electrode on the TS properties was presented here. The increasing r causes it to take much longer to discharge the charge stored in the HV cable and the tail of the current pulse can thus be longer than several tens of μs . This additional resistor r enables us to merge the characteristics of TS and GD together, i.e. relatively high current pulses ($\sim 1 \text{ A}$) with high efficiency of radical production are followed by long periods with the current above 1 mA during which plasma reaches characteristics typical for GD. Our further research in this area will be focused on scaling up the TS discharge to produce larger volumes of non-equilibrium air plasma and to reduce the power budget.

Acknowledgments

Effort sponsored by the AFOSR, Air Force Material Command, USAF, under grant FA8655-09-1-3110, Slovak Research and Development Agency APVV SK-FR-0038-09, and Slovak grant agency VEGA, under grants 1/0293/08 and 1/0668/10.

References

- [1] Civitano L 1993 *Non-Thermal Plasma Techniques for Pollution Control (NATO Series vol 1)* (New York: Springer)
- [2] Joshi A A, Locke B R, Arce P and Finney W C 1995 *J. Hazardous Mater.* **41** 3
- [3] Laroussi M 2002 *IEEE Trans. Plasma Sci.* **30** 1409
- [4] Pawlat J, Hensel K and Ihara S 2005 *Acta Phys. Slovaca* **55** 479
- [5] Machala Z, Janda M, Hensel K, Jedlovský I, Leštinská L, Foltin V, Martišovič V and Morvová M 2007 *J. Mol. Spectrosc.* **243** 194
- [6] Cernak M, Rahel J, Kovacik D, Simor M, Brablec A and Slavicek P 2004 *Contrib. Plasma Phys.* **44** 492
- [7] Loeb L B 1965 *Electrical Coronas, Their Basic Physical Mechanisms* (Berkeley, CA: University of California Press)
- [8] Kulikovskiy A A 1997 *IEEE Trans. Plasma Sci.* **25** 439
- [9] Raether H 1964 *Electron Avalanches and Breakdown in Gases* (London: Butterworths)
- [10] Kobayashi A, Osaki K and Yamabe C 2002 *Vacuum* **65** 475–9
- [11] Bromberg L, Cohn D R, Rabinovich A and Alexeev N 1999 *Int. J. Hydrogen Energy* **24** 1131–7
- [12] Kanzawa A 1993 *Plasma Sources Sci. Technol.* **2** 58–62

- [13] Efremov N M, Adamiak B Y, Blochin V I, Dadashev S J, Dmitriev K I, Gryaznova O P and Jusbashev V F 2000 *IEEE Trans. Plasma Sci.* **28** 238
- [14] Kogelschatz U 2003 *Plasma Chem. Plasma Process.* **23** 1
- [15] Wagner H-E, Brandenburg R, Kozlov K V, Sonnenfeld A, Michel P and Behnke J F 2003 *Vacuum* **71** 417
- [16] Mizuno A, Clements J S and Davis R H 1986 *IEEE Trans. Ind. Appl.* **22** 516–22
- [17] Lowke J J and Morrow R 1995 *IEEE Trans. Plasma Sci.* **23** 661–71
- [18] Penetrante B M, Bardsley J N and Hsiao M C 1997 *Japan. J. Appl. Phys.* **36** 5007–17
- [19] Masuda S and Nakao H 1990 *IEEE Trans. Ind. Appl.* **26** 374–83
- [20] Walsh J L, Shi J J and Kong M G 2006 *Appl. Phys. Lett.* **89** 161505
- [21] Pancheshnyi S V, Lacoste D A, Bourdon A and Laux C O 2006 *IEEE Trans. Plasma Sci.* **34** (part 1) 2478–87
- [22] Pai D, Lacoste D A and Laux C O 2008 *IEEE Trans. Plasma Sci.* **36** (part 1) 974–5
- [23] Pai D, Stancu G D, Lacoste D A and Laux C O 2009 *Plasma Sources Sci. Technol.* **18** 045030
- [24] Pilla G, Galley D, Lacoste D A, Lacas F, Veynante D and Laux C O 2006 *IEEE Trans. Plasma Sci.* **34** 2471
- [25] Machala Z, Morvová M, Marode E and Morva I 2000 *J. Phys. D: Appl. Phys.* **33** 3198
- [26] Akishev Y, Goossens O, Callebaut T, Leys C, Napartovich A and Trushkin N 2001 *J. Phys. D: Appl. Phys.* **34** 2875–82
- [27] Machala Z, Jedlovský I and Martišovič V 2008 *IEEE Trans. Plasma Sci.* **36** (part 1) 918–19
- [28] Akishev Y S, Deryugin A A, Kochetov I V, Napartovich A P and Trushkin N I 1993 *J. Phys. D: Appl. Phys.* **26** 1630–7
- [29] Machala Z, Jedlovský I, Chládeková L, Pongráč B, Gierl D, Janda M, Šikurová L and Polčič P 2009 *Eur. Phys. J. D* **54** 195
- [30] Bastien F and Marode E 1979 *J. Phys. D: Appl. Phys.* **12** 249
- [31] Marode E, Goldman A and Goldman M 1993 *Non-Thermal Plasma Techniques for Pollution Control (NATO ASI series, Part A) High pressure discharge as a trigger for pollution control* (Berlin: Springer) pp 167–90
- [32] Hafez R, Samson S and Marode E 1995 A prevented spark reactor for pollutant control investigation of no_x removal 12th ISPC (Minneapolis, MN, 21–25 August) ed J V Heberlein *et al* pp 855–61
- [33] Akishev Yu, Grushin M, Karalnik V, Petryakov A and Trushkin N 2010 *J. Phys. D: Appl. Phys.* **43** 075202
- [34] Janda M, Niklová A, Martišovič V and Machala Z 2010 Transient spark—dc driven nanosecond pulsed discharge in atmospheric air HAKONE XII (Trencianske Teplice, Slovakia, 12–17 September, 2010) pp 69–73
- [35] Janda M, Martišovič V, Morvová M, Machala Z and Hensel K 2007 *Eur. Phys. J. D* **45** 309
- [36] Naidis G V 2009 *Eur. Phys. J. Appl. Phys.* **47** 22803
- [37] Janda M, Machala Z and Laux C O 2009–2010 *Acta Physica Universitatis Comenianae* **L-LI** 85–93